

5. Investigation of atomic order-disorder in the $\text{La}_2\text{Zr}_2\text{O}_7$ pyrochlore under low energy (500 keV, Kr^{2+}) ion irradiation

5.1 Introduction

Creating and designing innovative materials for a wide range of engineering applications is of utmost importance [2]. The capability of developed materials for applications in diverse field depends on the response of materials to severe environments [2]. The engineering of disordering/ordering in cation and anion sub-lattices is particularly important in developing high-performance materials for advanced nuclear energy and high-temperature electrolytes system [2,3].

Pyrochlore matrices, $\text{A}_2\text{B}_2\text{O}_7$, with more than 500 synthetic compositions have a wide range of chemistry [4]. Unique physical and chemical properties of isometric $\text{A}_2\text{B}_2\text{O}_7$ pyrochlore materials make them an interesting candidate for the potential applications in various technological fields such as immobilization of radioactive nuclear waste, high-temperature solid electrolytes, superconductors, photoluminescence, piezoelectricity, catalysis, spin liquids, and so on [4]. Especially, the unique structural characteristic of $\text{A}_2\text{B}_2\text{O}_7$ compounds is the occurrence of disordering in cation and anion sub-lattices together [5].

Several previous studies found that the ionic and electronic conductivity depends on the degree of induced disordering in cation and anion sub-lattices [2,3,6]. Ou et al. stated that the oxygen ion conductivity of mixed-phase $\text{La}_2\text{Zr}_2\text{O}_7$ (LZO) is significantly enriched (400 times higher) than the conventional system [7]. Moreover, Saitzek et al. reported that the structural disorder-induced ferroelectricity in the $\text{La}_2\text{Zr}_2\text{O}_7$ [8].

Hence, inspired by the literature, an effort has been attempted to evaluate the structural alteration, i.e., the cation-anion disordering of LZO upon irradiation of 500 keV Kr^{2+} ions at 300 K and 88 K.

5.2 Results and Discussion

5.2.1 FE-SEM analysis

The surface texturing and grain size of the pristine (un-irradiated) $\text{La}_2\text{Zr}_2\text{O}_7$ (LZO) sample were examined from the FE-SEM. Fig. 5. 1 (a) shows the FE-SEM micrographs of the un-irradiated LZO sample. The grain sizes of the sample were determined using the rectangular intercept technique which has been explained in chapter 3 in the section of FE-SEM analysis.

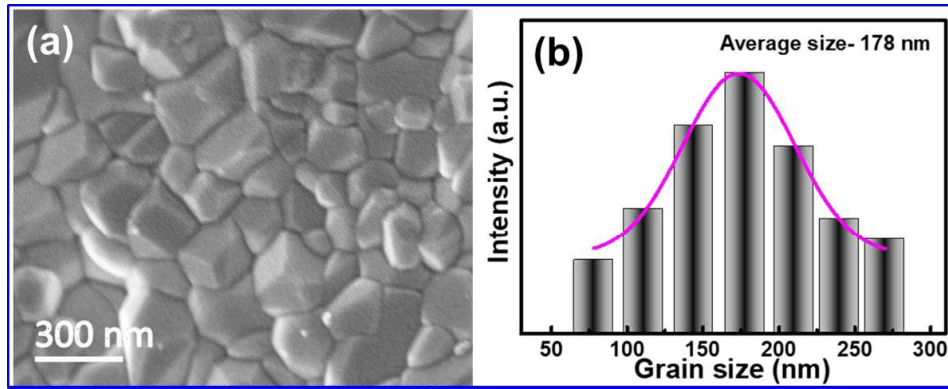


Figure 5.1 FE-SEM micrograph (a) and (b) size distribution histogram of un-irradiated LZO sample.

Fig. 5. 1 (a) exhibits that both the grain sizes and grain boundaries are well perceptible. The grain sizes over the range of 75-275 nm were deduced. The Gaussian fitting size histogram of the LZO sample is presented in Fig. 5. 1 (b) and the average grain size was found to be 178 nm.

5.2.2 GIXRD analysis

To evaluate the ordering/disordering of LZO samples upon irradiation of low-energy ions, the GIXRD technique has been employed. The GIXRD patterns of un-irradiated and irradiated LZO samples with the intensification of ion fluence are illustrated in Fig. 5.2 (a, b). Fig. 5.2 (a, b) exhibits the two different types series of reflections namely: (a) the reflections $\{(222), (400), (440)\}$ with the intense and sharp intensity and (b) the reflections $\{(111), (331), \text{and } (511)\}$ with the deficient intensity. The even miller indices reveal the fluorite structure, whereas the presence of odd miller indices specifies the cubic pyrochlore structure of $A_2B_2O_7$ compounds. The detection of superstructure reflections is arduous due to the deficient intensities of these reflections.

To compute the superstructure reflections, the magnified view of superstructure reflections of before and after irradiated LZO samples are illustrated in Fig. 5. 2 (c, d). Fig. 5. 2 (c, d) reveals the presence of superstructure reflections. The presence of superstructure reflections in all samples at both the temperatures specifies the formation of the pyrochlore phase and was found to be corroborated with the earlier studies of the LZO [9,10]. Further, Fig. 5. 2 (c, d) apparently suggests that the intensity of superstructure reflections decreases with the augmentation of fluence.

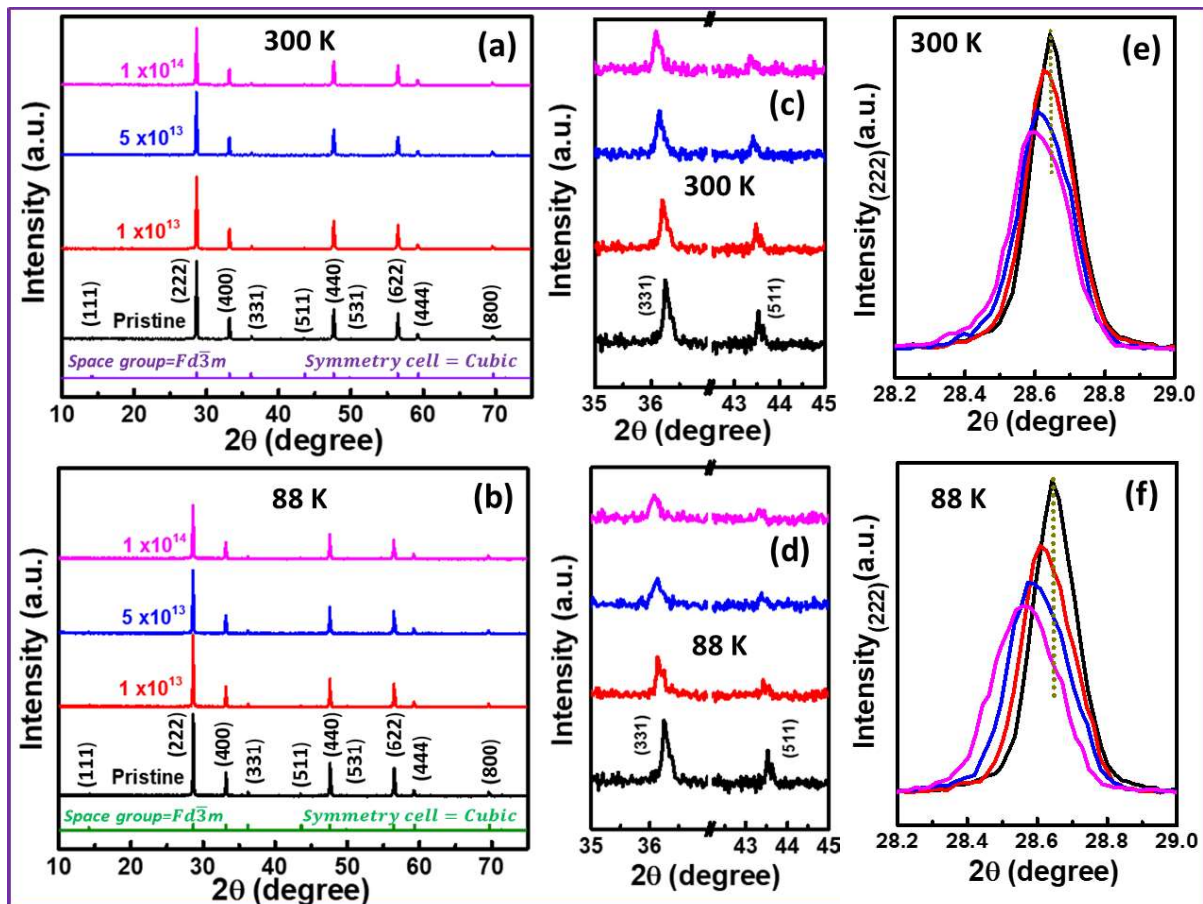


Figure 5.2 GIXRD patterns of LZO (a, b); enlarged view of (331), and (511) reflections and (c-d) magnified of (222) reflection.

The prudent evaluation of superstructure reflections of LZO samples shows that the reduction in the intensity of superstructure reflections is relatively pronounced at ~88 K than 300 K [Fig. 5. 2 (c, d)], which indicates that at a lower temperature (~88 K), the deterioration of the periodic ordering of crystal structure is comparatively prominent. The relatively prominent deterioration of periodic ordering of LZO samples irradiated at ~ 88 K may be correlated with the immovable nature of defects at low temperature [1,11]. Meanwhile, evaluating the intensity of superstructure reflections of LZO samples [Fig. 5. 2 (c, d)], it is noticed that at both the temperature, the reflections shift to lower 2θ with the enhancement of fluence.

To unearth the peak shifting, we plotted the enlarged view of high intense (222) reflection, which is shown in Fig. 5. 2 (e, f). Fig. 5. 2 (e, f) evidently shows the shifting of reflections towards lower 2θ with the enrichment of ion fluence. Here, it should be pointed out that the shifting of reflections towards lower 2θ specifies the engineering of lattice swelling;

namely the lattice constant of irradiated LZO samples at both the temperatures increases with augmentation of fluence. These results are corroborated with the earlier studies [12,13]. Moreover, to compute the impact of low energy ion irradiation (500 keV, Kr^{2+}) on the crystallinity of LZO samples, we quantified the full width at high maximum (FWHM) and intensity of most intense (222) reflection and presented in Fig. 5.3 (a-b). Fig. 5.3 (a-b) shows the variation of FWHM and intensity of (222) reflection. It is found that the FWHM increases and intensity declines with the function of fluence.

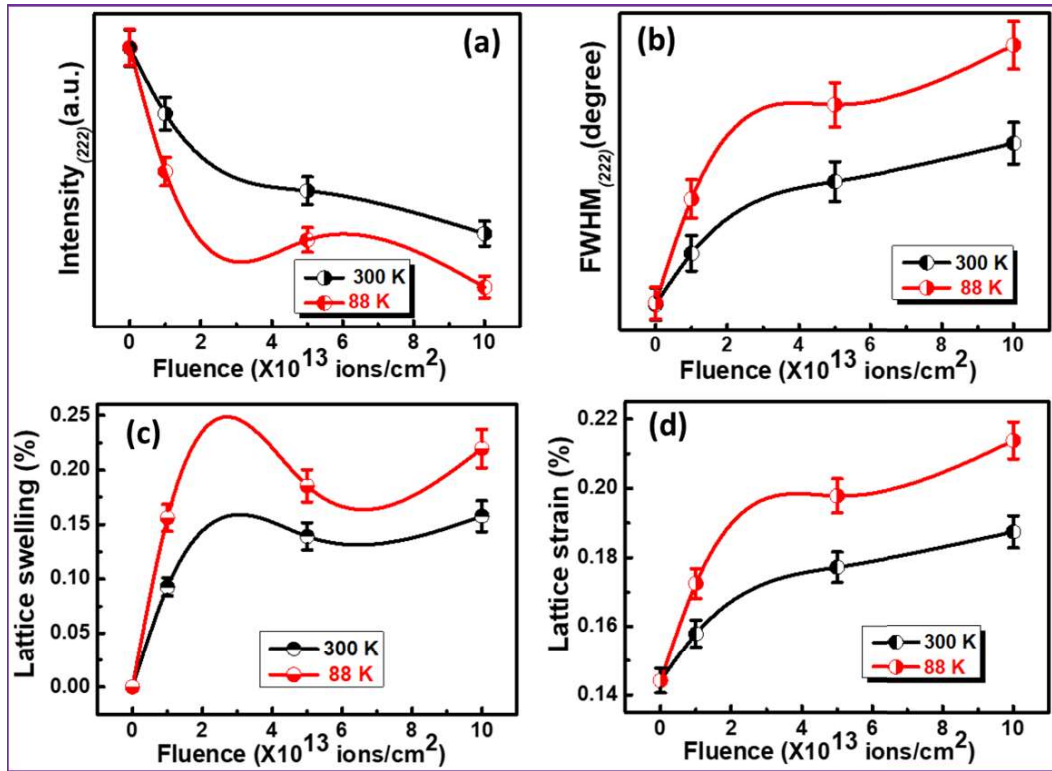


Figure 5.3 Representation of (a) intensity, (b) FWHM, (c) lattice swelling, and (d) strain of LZO samples in respect of ion fluence.

Here, we would like to stress that the concurrent enhancement in FWHM and decrement in the intensity of LZO reflections specify that the disordering of cations sub-lattice or/and deterioration of crystal structure enhanced with ion fluence. However, the concurrent enhancement in FWHM and decrement in the intensity of (222) reflection is found to be relatively more pronounced at ~ 88 K in respect of 300 K, i.e., the disordering of cations sub-lattice or/and deterioration of crystal structure is relatively higher at ~ 88 K than 300 K [11,14].

Here, it is worth mentioning that at low temperature the defects are immovable whereas defects become mobile at room temperature as per previous studies [15]. The relative higher deterioration of crystal structure may be correlated with the immobility of defects at ~ 88 K. Several earlier studies [6,13,16–19] have reported the broadening and weakening of reflection

due to applied pressure and ion irradiation, i.e., external parameters induced the disordering in the materials.

As we discussed above, the peaks shift towards to lower 2θ with the augmentation of fluence, which leads to lattice swelling [Fig. 5.2 (e-f)]; the enhancement in the lattice constants. Fig. 5.3 (c) shows the variation of lattice swelling in respect of fluence. The relatively higher lattice swelling is observed at ~ 88 K than 300 K.

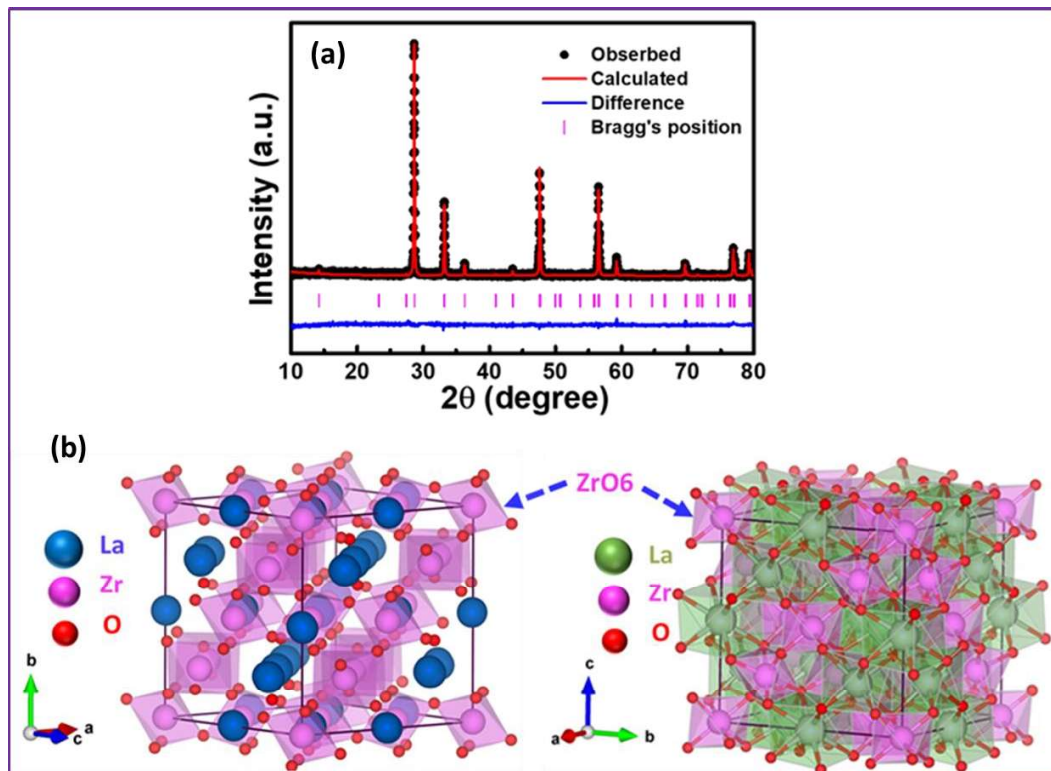


Figure 5.4 Rietveld refinement of pristine LZO (a) and representation of crystal structure of LZO, produced from the CIF file.

Moreover, we calculated the lattice strain employing the W-H method (described in the experiment section of chapter 2), and deduced lattice strain is presented in Fig. 5.3 (d). It is well recognized that strain engineering is an interesting feature to alter the properties of compounds. The lattice strain appears due to the presence/emergence of defects and dislocations in the materials by several methods: chemical substitution, applied pressure, ion irradiation, and so on [20,21]. Here, we wish to express that the variation of lattice strain is relatively higher with the function of fluence at ~ 88 K, which suggests that the distortion of lattice/crystallinity (induced defects) is substantially sublime at ~ 88 K than that of 300 K.

Chaudhary et al. reported that the induced disordering/defects generate the short-range stress field and result in, development of the stain in the lattice [22]. Qin et al. reported that the defects induced stress field not only originates the lattice strain; albeit also engenders lattice

expansion. Further, Qin et al. stated that the lattice strain and lattice constants have an inherent correlation with each other [23].

5.2.3 Rietveld refinement analysis

Using the FullProf program, the Rietveld refinement of the pre and post irradiated LZO samples was performed [24,25]. Fig. 5.4 (a) illustrates the refined XRD patterns of pristine LZO samples. The crystal structure of LZO was extracted from the CIF file and presented in Fig. 5.4 (b). The refined lattice constant of pristine LZO samples is found to be 10.786 Å.

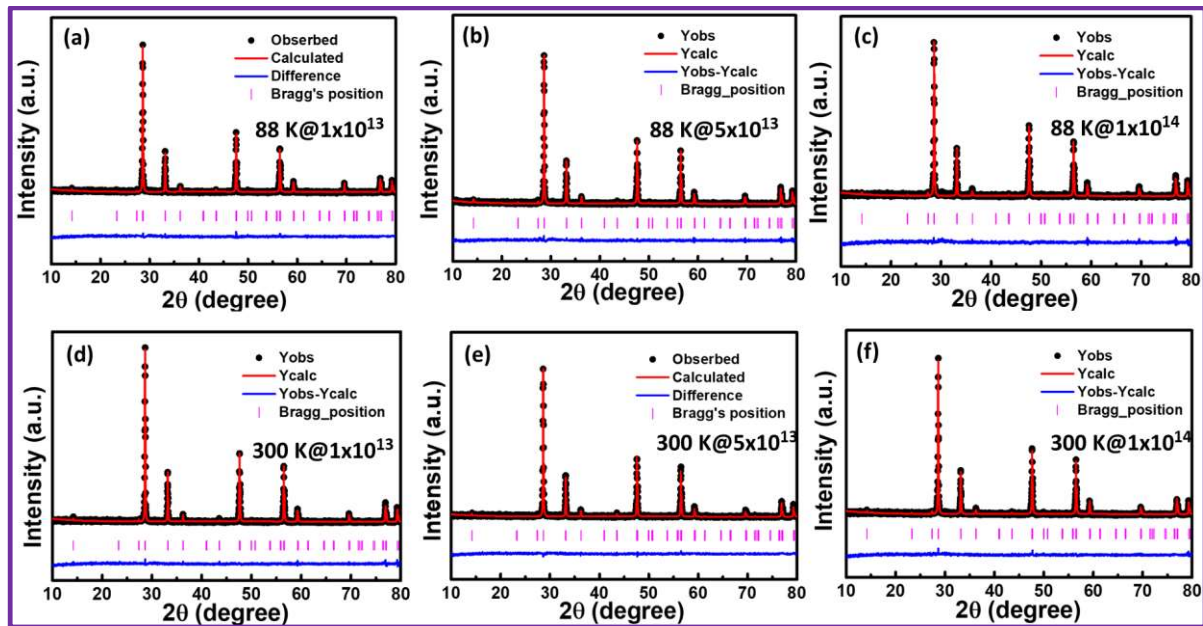


Figure 5.5 Refined GIXRD patterns of LZO (a-c) low temperature (88 K) and (d-f) 300 K.

Rietveld refinement of irradiated LZO samples at low temperature (88 K) and 300 K are shown in Figure 5.5. The Pseudo-Voigt function was employed for refining all LZO samples. The structural parameters deduced from the Rietveld refinement of GIXRD patterns of LZO samples are tabulated in Table 5.1. As we have mentioned above, the lattice strain and lattice constants have an inherent correlation in polycrystalline materials. It should be pointed out that the lattice strain shows the monotonic enhancement with fluence at low temperature (88 K) and room temperature (300 K) [Fig. 5.3 (d)] and assume the similar dependence of lattice constants on fluence at both temperatures. Table 5.1 signifies that the lattice constant enhances at both temperatures with the augmentation of fluence. It is observed that the enhancement in lattice constant at low temperature (88 K) is relatively higher than 300 K.

Here, we wish to stress that the GIXRD analysis of post irradiated LZO samples demonstrated that the lattice swelling is significantly higher for low temperature (88 K). The enhancement of the lattice constants of irradiated LZO samples, quantified from the Rietveld

refinement strengthens the GIXRD results. Yang et al. stated that the lattice swelling phenomenon is induced upon ion irradiation of light energy ions (400 keV, Ne²⁺), i.e., the lattice constant increased upon ion irradiation due to induced lattice swelling phenomenon with the augmentation of ion fluence [13]. Similarly, Li et al. reported the augmentation in lattice constant of Gd₂Ti₂O₇ with the enhancement of fluence [12].

Table 5.1 Structural parameters of pre and post-irradiated LZO samples.

	88 K				300 K			
	Pristine	1x10 ¹³	5x10 ¹³	1x10 ¹⁴	Pristine	1x10 ¹³	5x10 ¹³	1x10 ¹⁴
a_0	10.786	10.803	10.806	10.808	10.786	10.796	10.801	10.803
R_B	7.87	8.76	9.25	8.46	8.57	9.19	10.49	11.23
R_{wp}	12.01	11.09	11.23	12.29	11.32	13.42	11.32	12.20
R_{exp}	8.48	8.83	9.17	9.91	9.18	8.97	8.98	10.34
χ^2	1.41	1.25	1.22	1.24	1.23	1.49	1.26	1.18

Fig. 5.6 (a) shows the lattice expansion, i.e., cell volume expansion dependence on fluence at 88 K and 300 K. A monotonous dependence of cell volume on the fluence is observed and cell volume enhances with augmentation of fluence. It is noteworthy that the weakened reflections and lattice swelling/expansion indicate an order-disorder phenomenon upon ion irradiation [12,13]. Previous studies reported that there is a large difference in the X-ray scattering factors between both the cations (La³⁺ and Zr⁴⁺). Therefore, the cationic disorder of LZO samples can be quantified from the Rietveld refinement of the recorded GIXRD patterns [5,6].

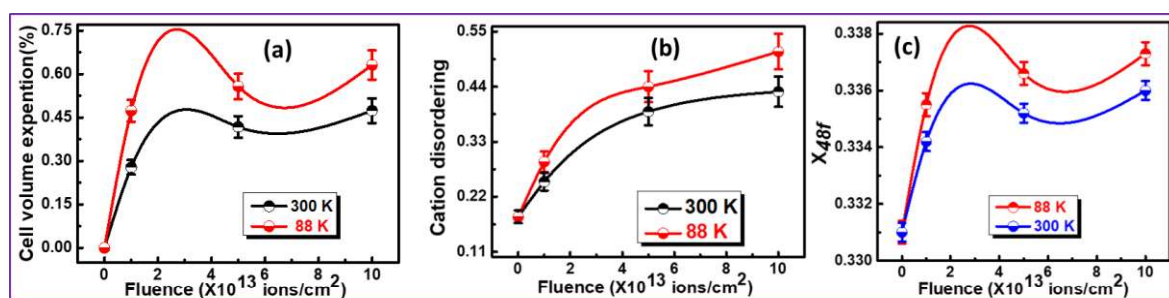


Figure 5.6 (a-c) Dependence of cell volume expansion, cation disordering, and (c) X_{48f} on fluence at 88 K and 300 K.

The cation order/disorder can be deduced from the cationic order/disorder parameter (Φ) and it can be represented as $\Phi=2\beta-1$ [5,6]. If Φ is equal to unity, the pyrochlore structure is referred to as an ordered pyrochlore structure. When β is equal to 0.5 ($\Phi=0$) a disordered fluorite structure is formed. We quantified the cation disorder at low temperature (88 K) and

room temperature with the function of fluence. A monotonous dependence of cation disorder on the fluence is observed, It is worth mentioning that pyrochlore structures possess intrinsic disorder [5,26–28]. It is reported that the LZO possesses lower than ~ 20 % cationic disorder and with the enhancement of applied field, disordering increased up to 55 % [6]. Fig. 5.6 (b) displays the variation of cation disorder with the function fluence and it reveals that the disordering of cation in pristine LZO sample is ~16 % which corroborated with the earlier studies [5,6].

Further, Fig. 5.6 (b) reveals that the cation disordering depends on irradiation temperature and fluence. As expected, cation disordering at low temperature (88 K) is relatively higher with the augmentation of fluence. The cation disordering is found to be 0.42 and 0.51 at 300 K and 88 K for the highest fluence (1.0×10^{14} ions/cm²). In addition, the disordering of anionic sub-lattice and vacancies also derived an important role in altering the structural characteristics and as well as electronic conductivity [2,7,29]. The 48f oxygen positional parameter, x_{48f} , specifies the crystal structure of pyrochlore compounds [3]. For example, when $x=0.375$, in this case, pyrochlore compounds have an ideal fluorite structure. If $x=0.3125$, the pyrochlore compounds possess an ordered pyrochlore structure [30–33].

As we know, the oxygen positional parameter, x_{48f} , determines the deviation of crystal structure. We quantified the x_{48f} parameter and plotted it with the function of fluence as illustrated in Fig. 5.6 (c). Fig. 5.6 (c) shows that the deduced value of the x_{48f} parameter for the pristine LZO sample is ~0.331 and corroborated with previously reported values of the x_{48f} parameter for LZO [34]. Moreover, the x_{48f} parameter enhances monotonically with the function of ion fluence [Fig. 5.6 (c)]. The value of the x_{48f} parameter at 88 K is found to be higher for similar fluence than at 300 K. The relatively higher value of the x_{48f} parameter at 88 K may be associated with the relatively more pronounced disordering/defects at 88 K [11]. Previous studies reported that the enhancement in the x_{48f} parameter signifies the enhancement of disorder in the system [33–35]. In addition, it should be noted that the augmentation in the x_{48f} parameter is significantly higher for initial fluence in comparison of successive higher fluence [Fig. 5.6 (c)].

The concurrent enhancement in cation disorder and x_{48f} parameter seems associated with augmentation of fluence. Here, we wish to stress that both cation disorder and x_{48f} parameter are relatively higher at 88 K than 300 K. The relative higher value of cation disorder and the x_{48f} parameter at 88 K signifies more pronounced disordering in cation and anion sub-lattices. These results suggest that the irradiation temperature plays a vital role in the variation of both parameters, i.e., cation disordering and x_{48f} parameter [1,11].

Zhang et al. stated that the dynamic recovery process (defect migration and clustering) becomes more active when irradiation is executed at a relatively higher temperature [36]. The small variation in the irradiation temperature significantly influences the recombination/recovery rates, i.e., ordering/disordering alter accordingly. Schrempel et al. found that the critical amorphization dose is significantly lower at 15 K than 300 K [1] due to the immovable nature of irradiation-induced defects at low temperature [1]. Velisa et al. found that the irradiation executed at 300 K induced the defects in the materials, while irradiation performed at 16 K produced the defects and fraction of amorphization due to suppression of defects recovery rates [11].

Based on the above discussion, we conclude that the fluence and irradiation temperature alter the degree of disordering in LZO samples, i.e., the ion irradiation-induced structural modifications exhibit dependence on the fluence and irradiation temperature. The relatively more pronounced broadened and weakened reflections of LZO at 88 K than 300 K seem associated with the immobile nature of defects.

5.2.4 Raman analysis

To obtain the extant information about the distortion in crystal structure or/and disordering in the LZO, the room temperature Raman spectroscopy was performed. Raman spectroscopy is a non-destructive technique for the characterization of materials. More detail about the Raman spectroscopy is explained in the characterization section of chapter 2. As per the group theory predictions and several experimental studies, the pyrochlore structure displays six Raman active vibrational modes [20,37–40]. Fig. 5.7 displays the Raman spectra of LZO before and after irradiation in the range of 100-700 cm^{-1} . Here, we wish to stress that the post-irradiation Raman spectra do not exhibit anomalous variation except relative reduction in the intensity and augmentation in the FWHM. The Raman modes significantly became broadened and weakened with the augmentation of fluence from 1.0×10^{13} to 1.0×10^{14} ions/ cm^2 . Upon higher irradiation fluence, the higher frequencies vibrational mode reduced significantly [Fig. 5.7 (a-b)]. It is observed that the reduction of the vibrational modes is relatively higher at 88 K than 300 K. The concurrent decrement in the intensities and broadening in the FWHM of Raman active vibrational modes are in accordance with the previous studies [26,41–43]. Moreover, we deconvoluted Raman spectra of the LZO sample for the irradiation fluence of 1.0×10^{13} ions/ cm^2 [Fig. 5.7 (c-d)].

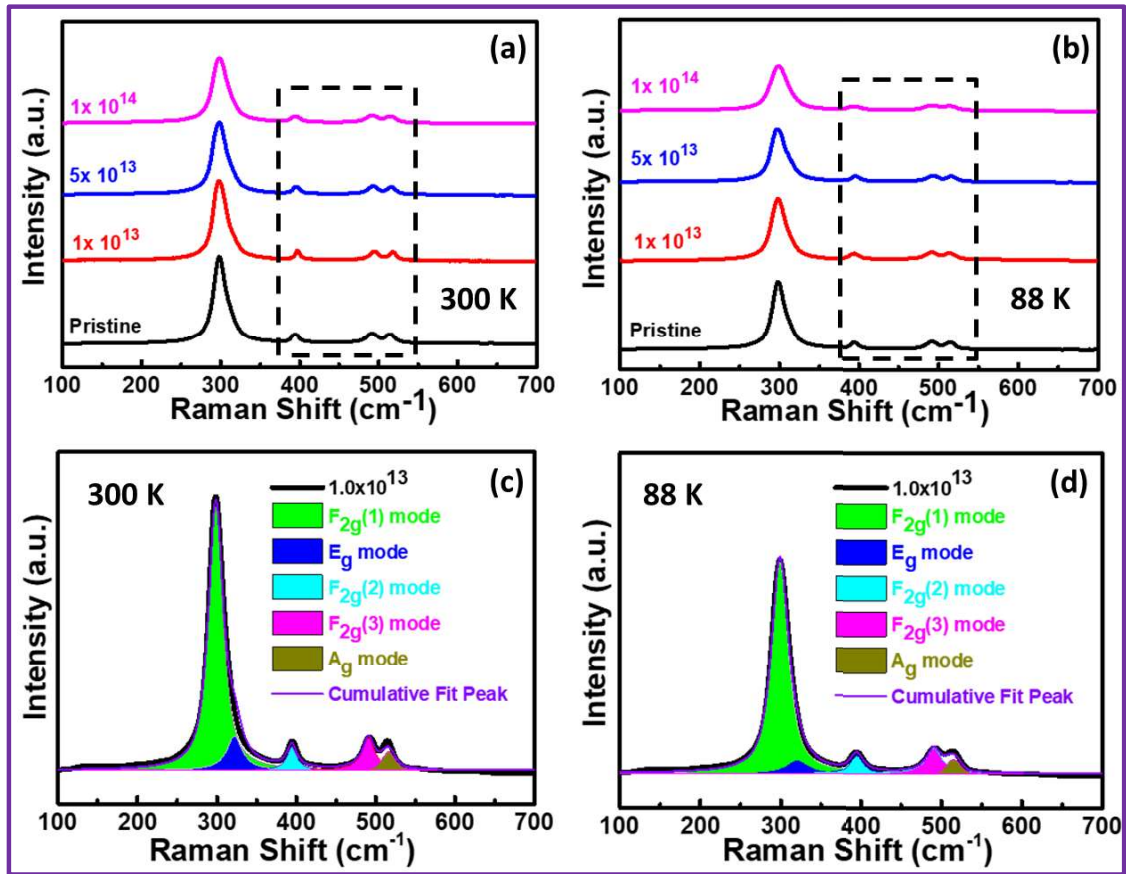


Figure 5.7 Raman spectra of LZO (a) 300 K, (b) 88 K, and (c-d) deconvoluted Raman spectra of LZO.

The deconvoluted Raman spectra show the presence of five Raman active vibrational modes situated at ~ 298.69 ($F_{2g}(1)$), 323.84 (E_g), 394.65 ($F_{2g}(2)$), 491.39 ($F_{2g}(3)$), and 515.00 (A_g). The Raman modes, $F_{2g}(1)$ and E_g are associated with B-O stretching and O-B-O bending vibrations. The two F_{2g} modes ($F_{2g}(2)$ and $F_{2g}(3)$) are related to A-O and B-O stretching and bending modes vibrations. The A_{1g} mode is associated with A-O stretching vibration [43–46]. Fig. 5.8 displays the schematic diagram representation of La-O and Zr-O modes with bending and stretching vibrations. The corresponding vibrational mode frequencies and assigned modes are displayed in Table 5.2. It is observed that there is a slight variation in the frequencies of vibration modes of before and after irradiated LZO samples. Here, it is worth mentioning that the slight variation in the frequencies of vibration modes may be associated with stressed lattice crystal upon ion irradiation [40,47].

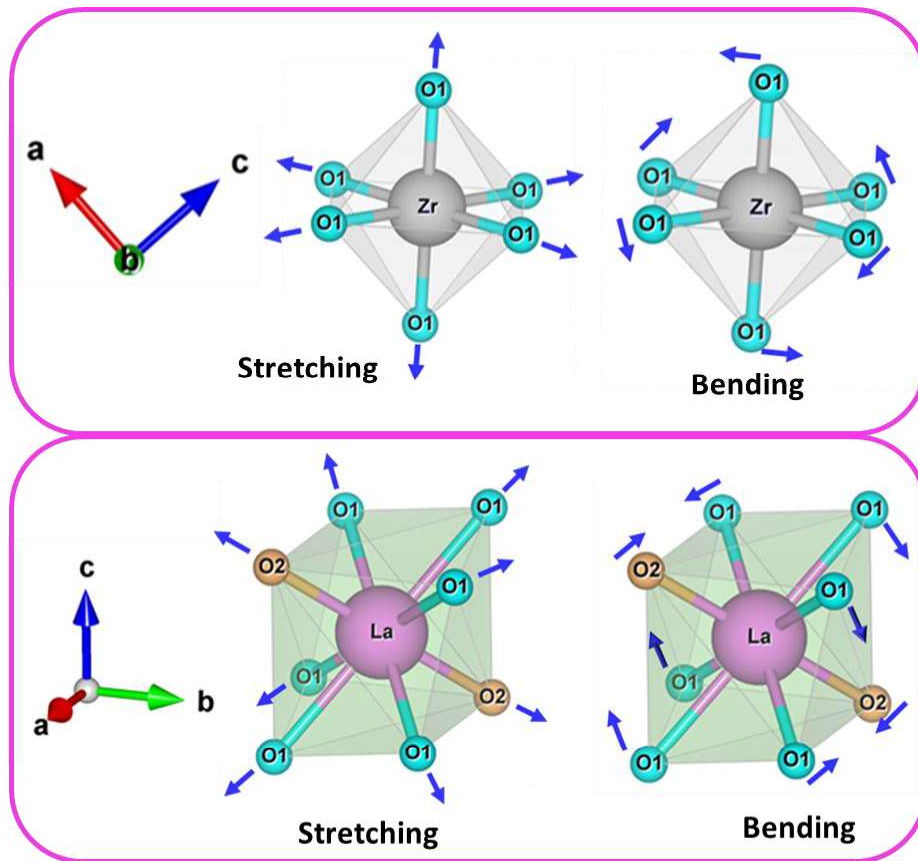


Figure 5.8 Illustration of bending and stretching vibrations in LZO samples.

Table 5.2 Raman frequencies and assigned modes of LZO samples before and after irradiation.

<i>Pristine</i>	<i>Room temperature</i>			<i>Low temperature</i>			<i>Assigned mode</i>
	1.0×10^{13}	5.0×10^{13}	1.0×10^{14}	1.0×10^{13}	5.0×10^{13}	1.0×10^{14}	
298.69	298.75	298.46	298.71	298.58	298.28	299.05	$F_{2g}(1)$
323.84	322.07	324.48	321.47	323.49	321.41	326.58	E_g
394.65	397.82	396.19	395.31	394.31	396.46	394.74	$F_{2g}(2)$
491.39	494.54	492.75	491.86	491.144	492.7	492.1	$F_{2g}(3)$
515.00	518.2	516.84	515.02	514.58	517.46	516.85	A_g

In order to get further details about the lattice distortions/weakening and broadening of vibrational modes of LZO samples upon ion irradiation, we quantified the FWHM and intensity of vibrational modes. The quantified intensity and FWHM of vibrational modes at 88 K and 300 K is presented in Fig. 5.9 (a-b). Fig. 5.9 (a-b) evidently exhibits the intensity of the

vibrational modes at both the temperature decreases with the function of fluence. At the same time, the FWHM enhances with further enhancement of fluence. The weakening and broadening of vibration modes specify the distortion in the lattice, i.e., crystal lattice became stressed upon ion irradiation [45,47].

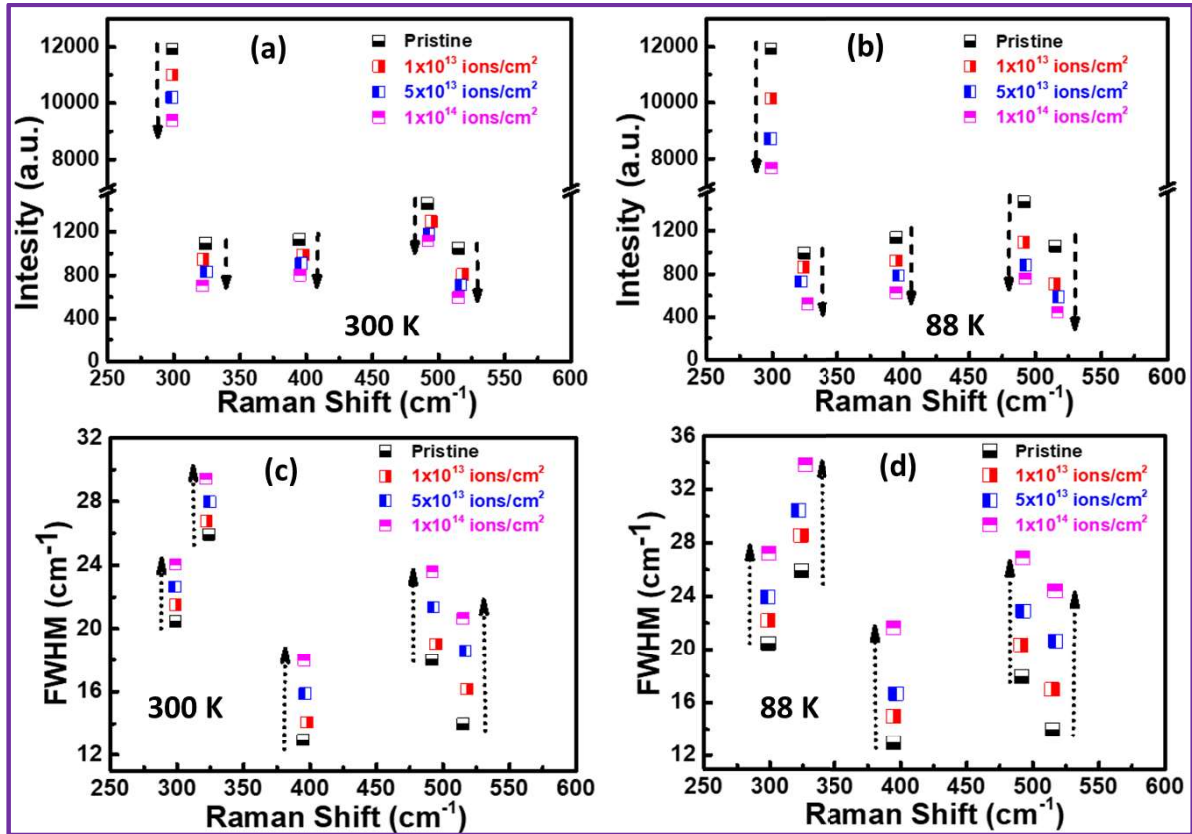


Figure 5.9 (a-d) Dependence of intensity and FWHM on fluence at 300 K and 88 K.

Previous studies reported the weakening and broadening in the vibrational modes due to distortion of chemical bonding upon ion irradiation [26,47]. In addition, the weakening and broadening of vibration modes, i.e., distortion of bonds (distortion in the crystal lattice) are found to be significantly higher for 88 K than 300 K [48]. These results signify that the deterioration of crystal lattice is more pronounced at 88 K than 300 K. In a similar way, Mandal et al. observed the weakening of vibrational modes due to induced distortion in the bonds [45].

It should be noted that the substitution of cations in pyrochlore oxides triggered the cation sub-lattice disorder and redistribution of anions among the O(1) and O(2), and 8*b* vacant position [37]. Moreover, the broadening and weakening of vibrational modes in pyrochlore oxides originated due to induced structural disorder upon substitution [35,37]. Zhang et al. stated that ion irradiation induces structural distortion in La₂Zr₂O₇ and results in, the vibrational modes become weakened and broadened [43].

As per the above discussion, in the present study, we conclude that the weakening and broadening of vibrational modes with augmentation of fluence are related to induced disorder in the LZO samples upon irradiation. The relatively much weaker and broaden vibrational modes at 88 K than 300 K may be related to the immobile nature of induced disorder/defects. The qualitative Raman spectroscopy results are corroborated with the GIXRD analysis.

5.3 Conclusion

To investigate the influence of light ion irradiation on structural modifications of LZO, the prepared LZO samples were irradiated at 88 K and 300 K using 500 keV Kr^{2+} ions with three different fluences. The before and after irradiation of LZO samples were studied using GIXRD and Raman spectroscopy techniques. The continuous weakening and broadening of LZO reflections with the enhancement of fluence shows the induced structural disordering at 88 K and 300 K upon irradiation and are relatively higher at a lower temperature (88 K). The lattice strain and cell volume expansion depend on the irradiation temperature and fluence; are significantly more pronounced at 88 K than 300 K. Disordering of cation and anion enhanced as a function of fluence and it is relatively higher at 88 K. Raman spectroscopy revealed the augmentation of disorder in LZO samples with the enrichment of fluence. Further, Raman spectroscopy analysis confirmed the higher disorder/distortion in the system at 88 K. Both, the XRD and Raman spectroscopy confirmed more pronounced structural modification (defects/disordering) in LZO samples at 88 K in comparison of 300 K due to the immobile nature of ion irradiation-induced disorder/defects. The structural transformations achieved here may be constructive for possible use in emerging applications such as thermal barrier coatings, catalysts, solid electrolytes, *etc.*

References

- [1] F. Schrempel, T. Gischkat, H. Hartung, E.-B. Kley, W. Wesch, Ion beam enhanced etching of LiNbO_3 , *Nucl. Instruments Methods Phys. Res. Sect. B Beam Interact. with Mater. Atoms.* 250 (2006) 164–168. <https://doi.org/10.1016/j.nimb.2006.04.101>.
- [2] F.X. Zhang, J.W. Wang, J. Lian, M.K. Lang, U. Becker, R.C. Ewing, Phase stability and pressure dependence of defect formation in $\text{Gd}_2\text{Ti}_2\text{O}_7$ and $\text{Gd}_2\text{Zr}_2\text{O}_7$ pyrochlores, *Phys. Rev. Lett.* 100 (2008) 2–5. <https://doi.org/10.1103/PhysRevLett.100.045503>.
- [3] J. Lian, L.M. Wang, S.X. Wang, J. Chen, L.A. Boatner, R.C. Ewing, Nanoscale manipulation of pyrochlore: New nanocomposite ionic conductors, *Phys. Rev. Lett.* 87 (2001) 3–6. <https://doi.org/10.1103/PhysRevLett.87.145901>.
- [4] R.C. Ewing, W.J. Weber, J. Lian, Nuclear waste disposal—pyrochlore ($\text{A}_2\text{B}_2\text{O}_7$): Nuclear waste form for the immobilization of plutonium and “minor” actinides, *J. Appl. Phys.* 95 (2004) 5949–5971. <https://doi.org/10.1063/1.1707213>.
- [5] F.X. Zhang, M. Lang, R.C. Ewing, Atomic disorder in $\text{Gd}_2\text{Zr}_2\text{O}_7$ pyrochlore, *Appl. Phys. Lett.* 106 (2015) 191902. <https://doi.org/10.1063/1.4921268>.
- [6] F.X. Zhang, M. Lang, Z. Liu, R.C. Ewing, Pressure-induced disordering and anomalous lattice expansion in $\text{La}_2\text{Zr}_2\text{O}_7$ pyrochlore, *Phys. Rev. Lett.* 105 (2010) 1–4. <https://doi.org/10.1103/PhysRevLett.105.015503>.
- [7] G. Ou, W. Liu, L. Yao, H. Wu, W. Pan, High conductivity of $\text{La}_2\text{Zr}_2\text{O}_7$ nanofibers by phase control, *J. Mater. Chem. A* 2 (2014) 1855–1861. <https://doi.org/10.1039/c3ta13465b>.
- [8] S. Saitzek, Z. Shao, A. Bayart, A. Ferri, M. Huvé, P. Roussel, R. Desfeux, Ferroelectricity in $\text{La}_2\text{Zr}_2\text{O}_7$ thin films with a frustrated pyrochlore-type structure, *J. Mater. Chem. C* 2 (2014) 4037–4043. <https://doi.org/10.1039/c4tc00207e>.
- [9] B. Paul, K. Singh, T. Jaroń, A. Roy, A. Chowdhury, Structural properties and the fluorite–pyrochlore phase transition in $\text{La}_2\text{Zr}_2\text{O}_7$: The role of oxygen to induce local disordered states, *J. Alloys Compd.* 686 (2016) 130–136. <https://doi.org/10.1016/j.jallcom.2016.05.347>.
- [10] A. Panghal, P.K. Kulriya, Y. Kumar, F. Singh, N.L. Singh, Investigations of atomic disorder and grain growth kinetics in polycrystalline $\text{La}_2\text{Zr}_2\text{O}_7$, *Appl. Phys. A Mater. Sci. Process.* 125 (2019) 1–11. <https://doi.org/10.1007/s00339-019-2720-8>.
- [11] G. Velişa, E. Wendler, L.L. Wang, Y. Zhang, W.J. Weber, Amorphization kinetics in strontium titanate at 16 and 300 K under argon ion irradiation, *J. Mater. Sci.* 54 (2019)

- 6066–6072. <https://doi.org/10.1007/s10853-018-03313-7>.
- [12] Y.H. Li, J. Wen, Y.Q. Wang, Z.G. Wang, M. Tang, J.A. Valdez, K.E. Sickafus, The irradiation effects of $\text{Gd}_2\text{Hf}_2\text{O}_7$ and $\text{Gd}_2\text{Ti}_2\text{O}_7$, *Nucl. Instruments Methods Phys. Res. Sect. B Beam Interact. with Mater. Atoms.* 287 (2012) 130–134. <https://doi.org/10.1016/j.nimb.2012.06.003>.
- [13] D. Yang, Y. Xia, J. Wen, J. Liang, P. Mu, Z. Wang, Y. Li, Y. Wang, Role of ion species in radiation effects of $\text{Lu}_2\text{Ti}_2\text{O}_7$ pyrochlore, *J. Alloys Compd.* 693 (2017) 565–572. <https://doi.org/10.1016/j.jallcom.2016.09.227>.
- [14] J. Lian, K.B. Helean, B.J. Kennedy, L.M. Wang, A. Navrotsky, R.C. Ewing, Effect of structure and thermodynamic stability on the response of lanthanide stannate pyrochlores to ion beam irradiation, *J. Phys. Chem. B.* 110 (2006) 2343–2350. <https://doi.org/10.1021/jp055266c>.
- [15] S. Thevuthasan, W. Jiang, V. Shutthanandan, W.J. Weber, Accumulation and thermal recovery of disorder in Au^{2+} -irradiated SrTiO_3 , *J. Nucl. Mater.* 289 (2001) 204–209. [https://doi.org/10.1016/S0022-3115\(00\)00699-1](https://doi.org/10.1016/S0022-3115(00)00699-1).
- [16] Y.H. Li, B.P. Uberuaga, C. Jiang, S. Choudhury, J.A. Valdez, M.K. Patel, J. Won, Y.Q. Wang, M. Tang, D.J. Safarik, D.D. Byler, K.J. McClellan, I.O. Usov, T. Hartmann, G. Baldinozzi, K.E. Sickafus, Role of antisite disorder on preamorphization swelling in titanate pyrochlores, *Phys. Rev. Lett.* 108 (2012) 1–5. <https://doi.org/10.1103/PhysRevLett.108.195504>.
- [17] Q.R. Xie, J. Zhang, D.M. Yin, Q.X. Guo, N. Li, Krypton ion irradiation-induced amorphization and nano-crystal formation in pyrochlore $\text{Lu}_2\text{Ti}_2\text{O}_7$ at room temperature, *Chinese Phys. B.* 24 (2015). <https://doi.org/10.1088/1674-1056/24/12/126103>.
- [18] K. Liu, K. Zhang, T. Deng, B. Luo, H. Zhang, Heavy-ion irradiation effects of $\text{Gd}_2\text{Zr}_2\text{O}_7$ nanocrystalline ceramics as nuclear waste immobilization matrix, *J. Nucl. Mater.* 538 (2020) 152236. <https://doi.org/10.1016/j.jnucmat.2020.152236>.
- [19] J. Niu, X. Wu, H. Zhang, S. Qin, Pressure-induced phase transition of $\text{La}_2\text{Zr}_2\text{O}_7$ and $\text{La}_{0.5}\text{Gd}_{1.5}\text{Zr}_2\text{O}_7$ pyrochlore, *RSC Adv.* 9 (2019) 18954–18962. <https://doi.org/10.1039/c9ra03438b>.
- [20] D.R. Rittman, K.M. Turner, S. Park, A.F. Fuentes, C. Park, R.C. Ewing, W.L. Mao, Strain engineered pyrochlore at high pressure, *Sci. Rep.* 7 (2017) 1–10. <https://doi.org/10.1038/s41598-017-02637-9>.
- [21] P. Scardi, M. Leoni, R. Delhez, Line broadening analysis using integral breadth methods: a critical review, *J. Appl. Crystallogr.* 37 (2004) 381–390. <https://doi.org/>

- 10.1107/S0021889804004583.
- [22] B. Choudhury, P. Chetri, A. Choudhury, Annealing temperature and oxygen-vacancy-dependent variation of lattice strain, band gap and luminescence properties of CeO₂ nanoparticles, *J. Exp. Nanosci.* 10 (2015) 103–114. <https://doi.org/10.1080/17458080.2013.801566>.
- [23] W. Qin, T. Nagase, Y. Umakoshi, J.A. Szpunar, Relationship between microstrain and lattice parameter change in nanocrystalline materials, *Philos. Mag. Lett.* 88 (2008) 169–179. <https://doi.org/10.1080/09500830701840155>.
- [24] Y. Kumar, A. Sharma, M.A. Ahmed, S.S. Mali, C.K. Hong, P.M. Shirage, Morphology-controlled synthesis and enhanced energy product (BH) max of CoFe₂O₄ nanoparticles, *New J. Chem.* 42 (2018) 15793–15802. <https://doi.org/10.1039/C8NJ02177E>.
- [25] Y. Kumar, P.M. Shirage, Highest coercivity and considerable saturation magnetization of CoFe₂O₄ nanoparticles with tunable band gap prepared by thermal decomposition approach, *J. Mater. Sci.* 52 (2017) 4840–4851. <https://doi.org/10.1007/s10853-016-0719-5>.
- [26] Q. Qing, X. Shu, D. Shao, H. Zhang, F. Chi, X. Lu, Irradiation response of Nd₂Zr₂O₇ under heavy ions irradiation, *J. Eur. Ceram. Soc.* 38 (2018) 2068–2073. <https://doi.org/10.1016/j.jeurceramsoc.2017.11.050>.
- [27] T. Subramani, A. Voskanyan, K. Jayanthi, M. Abramchuk, A. Navrotsky, A Comparison of Order-Disorder in Several Families of Cubic Oxides, *Front. Chem.* 9 (2021) 1–21. <https://doi.org/10.3389/fchem.2021.719169>.
- [28] D. Simeone, G.J. Thorogood, D. Huo, L. Luneville, G. Baldinozzi, V. Petricek, F. Porcher, J. Ribis, L. Mazerolles, L. Largeau, J.F. Berar, S. Surble, Intricate disorder in defect fluorite/pyrochlore: A concord of chemistry and crystallography, *Sci. Rep.* 7 (2017) 1–7. <https://doi.org/10.1038/s41598-017-02787-w>.
- [29] X.-L. Xia, Z.-G. Liu, J.-H. Ouyang, Y. Zheng, Preparation, Structural Characterization, and Enhanced Electrical Conductivity of Pyrochlore-type (Sm_{1-x}Eux)₂Zr₂O₇ Ceramics, *Fuel Cells.* 12 (2012) 624–632. <https://doi.org/10.1002/fuce.201200015>.
- [30] L. Kong, I. Karatchevtseva, D.J. Gregg, M.G. Blackford, R. Holmes, G. Triani, Gd₂Zr₂O₇ and Nd₂Zr₂O₇ pyrochlore prepared by aqueous chemical synthesis, *J. Eur. Ceram. Soc.* 33 (2013) 3273–3285. <https://doi.org/10.1016/j.jeurceramsoc.2013.05.011>.
- [31] R.C. Ewing, J. Lian, L.M. Wang, Ion beam-induced amorphization of the pyrochlore structure-type: A review, *Mater. Res. Soc. Symp. - Proc.* 792 (2003) 37–48. <https://doi.org/10.1557/proc-792-r2.1>.

- [32] T. HAGIWARA, K. NOMURA, H. KAGEYAMA, Crystal structure analysis of $Ln_2Zr_2O_7$ ($Ln=Eu$ and La) with a pyrochlore composition by high-temperature powder X-ray diffraction, *J. Ceram. Soc. Japan.* 125 (2017) 65–70. <https://doi.org/10.2109/jcersj2.16248>.
- [33] B.J. Kennedy, B.A. Hunter, C.J. Howard, Structural and Bonding Trends in Tin Pyrochlore Oxides, *J. Solid State Chem.* 130 (1997) 58–65. <https://doi.org/10.1006/jssc.1997.7277>.
- [34] J. Lian, X.T. Zu, K.V.G. Kutty, J. Chen, L.M. Wang, R.C. Ewing, R.C. Ewing, Ion-irradiation-induced amorphization of $La_2Zr_2O_7$ pyrochlore, *Phys. Rev. B - Condens. Matter Mater. Phys.* 66 (2002) 541081–541085. <https://doi.org/10.1103/PhysRevB.66.054108>.
- [35] B.P. Mandal, P.S.R. Krishna, A.K. Tyagi, Order–disorder transition in the $Nd_{2-y}Y_yZr_2O_7$ system: Probed by X-ray diffraction and Raman spectroscopy, *J. Solid State Chem.* 183 (2010) 41–45. <https://doi.org/10.1016/j.jssc.2009.10.010>.
- [36] Y. Zhang, J. Lian, C.M. Wang, W. Jiang, R.C. Ewing, W.J. Weber, Ion-induced damage accumulation and electron-beam-enhanced recrystallization in $SrTiO_3$, *Phys. Rev. B - Condens. Matter Mater. Phys.* 72 (2005) 1–8. <https://doi.org/10.1103/PhysRevB.72.094112>.
- [37] M. Glerup, O.F. Nielsen, F.W. Poulsen, The Structural Transformation from the Pyrochlore Structure, $A_2B_2O_7$, to the Fluorite Structure, AO_2 , Studied by Raman Spectroscopy and Defect Chemistry Modeling, *J. Solid State Chem.* 160 (2001) 25–32. <https://doi.org/10.1006/jssc.2000.9142>.
- [38] B.E. SCHEETZ, W.B. WHITE, Characterization of Anion Disorder in Zirconate $A_2B_2O_7$ Compounds by Raman Spectroscopy, *J. Am. Ceram. Soc.* 62 (1979) 468–470. <https://doi.org/10.1111/j.1151-2916.1979.tb19107.x>.
- [39] D. Michel, M.P. y Jorba, R. Collongues, Study by Raman spectroscopy of order-disorder phenomena occurring in some binary oxides with fluorite-related structures, *J. Raman Spectrosc.* 5 (1976) 163–180. <https://doi.org/10.1002/jrs.1250050208>.
- [40] S. Brown, H.C. Gupta, J.A. Alonso, M.J. Martinez-Lope, Vibrational spectra and force field calculation of $A_2Mn_2O_7$ ($A=Y, Dy, Er, Yb$) pyrochlores, *J. Raman Spectrosc.* 34 (2003) 240–243. <https://doi.org/10.1002/jrs.982>.
- [41] S. Park, C.L. Tracy, F. Zhang, R.I. Palomares, C. Park, C. Trautmann, M. Lang, W.L. Mao, R.C. Ewing, Swift-heavy ion irradiation response and annealing behavior of A_2TiO_5 ($A = Nd, Gd, \text{ and } Yb$), *J. Solid State Chem.* 258 (2018) 108–116. <https://doi.org/10.1016/j.ssc.2018.05.010>.

- org/10.1016/j.jssc.2017.09.028.
- [42] G. Sattonnay, S. Moll, L. Thomé, C. Decorse, C. Legros, P. Simon, J. Jagielski, I. Jozwik, I. Monnet, Phase transformations induced by high electronic excitation in ion-irradiated $\text{Gd}_2(\text{Zr}_x\text{Ti}_{1-x})_2\text{O}_7$ pyrochlores, *J. Appl. Phys.* 108 (2010) 103512. <https://doi.org/10.1063/1.3503452>.
- [43] S.X. Zhang, J. Liu, H. Xie, L.J. Xu, P.P. Hu, J. Zeng, Z.Z. Li, L. Liu, W.S. Ai, P.F. Zhai, Vibrational modes in $\text{La}_2\text{Zr}_2\text{O}_7$ pyrochlore irradiated with disparate electrical energy losses, *Chinese Phys. B.* 28 (2019). <https://doi.org/10.1088/1674-1056/ab43bf>.
- [44] L. Kong, I. Karatchevtseva, D.J. Gregg, M.G. Blackford, R. Holmes, G. Triani, A Novel Chemical Route to Prepare $\text{La}_2\text{Zr}_2\text{O}_7$ Pyrochlore, *J. Am. Ceram. Soc.* 96 (2013) 935–941. <https://doi.org/10.1111/jace.12060>.
- [45] B.P. Mandal, P.S.R. Krishna, A.K. Tyagi, Order-disorder transition in the $\text{Nd}_2\text{Y}_y\text{Zr}_2\text{O}_7$ system: Probed by X-ray diffraction and Raman spectroscopy, *J. Solid State Chem.* 183 (2010) 41–45. <https://doi.org/10.1016/j.jssc.2009.10.010>.
- [46] S. Wang, W. Li, S. Wang, Z. Chen, Synthesis of nanostructured $\text{La}_2\text{Zr}_2\text{O}_7$ by a non-alkoxide sol-gel method: From gel to crystalline powders, *J. Eur. Ceram. Soc.* 35 (2015) 105–112. <https://doi.org/10.1016/j.jeurceramsoc.2014.08.032>.
- [47] M. Zhou, C. Hou, Y. Xie, L. Wang, X. Shu, D. Shao, X. Lu, Alpha-radiation effects of $\text{Gd}_2\text{Zr}_2\text{O}_7$ bearing simulated multi-nuclides, *J. Aust. Ceram. Soc.* 55 (2019) 831–836. <https://doi.org/10.1007/s41779-018-00297-0>.
- [48] W.J. Weber, N.J. Hess, G.D. Maupin, Amorphization in $\text{Gd}_2\text{Ti}_2\text{O}_7$ and $\text{CaZrTi}_2\text{O}_7$ irradiated with 3 MeV argon ions, *Nucl. Instruments Methods Phys. Res. Sect. B Beam Interact. with Mater. Atoms.* 65 (1992) 102–106. [https://doi.org/10.1016/0168-583X\(92\)95021-I](https://doi.org/10.1016/0168-583X(92)95021-I).